Finite element analysis for Solder Ball Connect (SBC) structural design optimization

by J. S. Corbin

Solder Ball Connect (SBC) is a second-level surface mount electronics packaging technology in which ceramic modules containing one or more chips are joined to a circuit card (FR-4) by means of an array of nonhomogeneous solder columns. These columns consist of a high-temperature-melting 90%Pb/10%Sn solder sphere attached to the module and card with eutectic solder fillets. The solder structures accommodate the bulk of the strain (which is due to the thermal-expansion mismatch between FR-4 and the 9211 ceramic of the modules) generated during power cycling. If the solder structures are not properly designed, the thermal strain can be a source of premature fatigue failure. In this work, finite element analysis is used to characterize the plastic strains that develop in the SBC interconnection during thermal cycling. Since plastic strain is a dominant parameter that influences low-cycle fatigue, it is used as a basis of comparison for various structural alternatives. Designed experiment techniques are used to systematically evaluate the thermal strain sensitivity to structural variables. Results are used to identify an optimally reliable structure that is robust in terms of assembly-process variables.

Introduction

Solder Ball Connect (SBC) is a second-level assembly, surface mount interconnection technology in which multilayer ceramic (MLC) modules containing one or more chips are directly attached to FR-4 cards. The assembly process is described in detail by Banks et al. [1].

The SBC structure **(Figure 1)** consists of high-temperature-melting noneutectic solder balls (90%Pb/10%Sn, T_{melt} = 268–290°C) approximately 0.89 mm in diameter. These balls are attached to the modules (on molybdenum pads) and to the FR-4 card (on copper pads) with eutectic solder (63%Pb/37%Sn, T_{melt} = 183°C). The solder balls are arranged in a square array with a typical ball spacing of 1.27 mm (from center to center).

Module sizes range from approximately 18 mm square to 32 mm square, with a total input/output capability of 196 to 625. The first-level package, consisting of the multilayer ceramic module and attached solder balls, is surface-

mountable and compatible with existing surface mount technology assembly processes. Eutectic solder paste is deposited onto the pad array on the card by means of a screening process; the module and solder ball package is placed onto the pad array of the card; and the card/module assembly is reflowed by means of a vapor-phase or infrared process. A heat sink is optionally attached to the module cap after assembly of the module and the card.

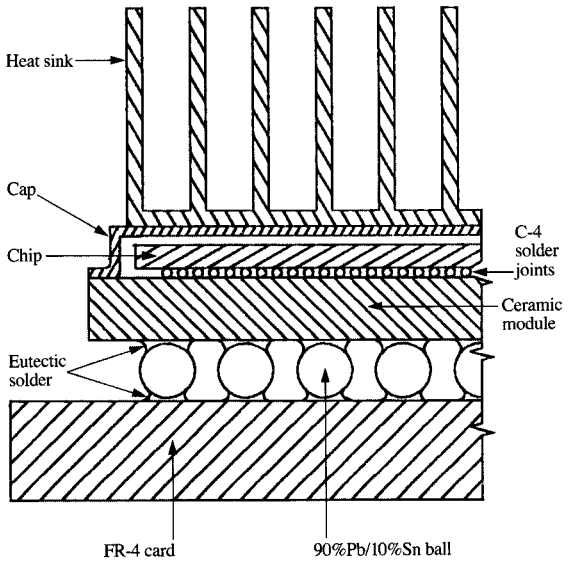

Figure 1

Solder Ball Connect configuration.

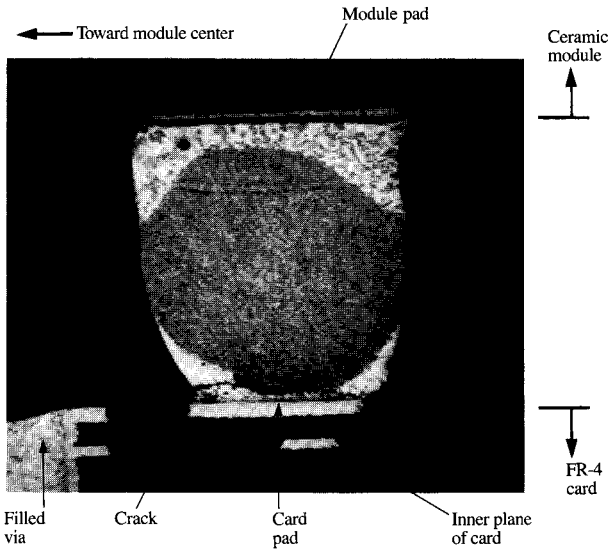

Figure 2

Typical SBC fatigue failure due to accelerated thermal cycling.

The reliability of devices operating in customer environments is a key concern in electronics packaging design. One aspect of reliability that is of particular importance to SBC technology is the potential premature fatigue failures that can occur in the solder joints. (In this paper we consider the solder "joint" to be the entire structure consisting of solder ball and eutectic solder at both card and module interfaces.) These fatigue failures are induced by the thermal expansion mismatch between the module ceramic (with coefficient of thermal expansion $\alpha = 7 \times 10^{-6}$/°C) and the FR-4 card (with coefficient of thermal expansion $\alpha = 20 \times 10^{-6}$/°C), which creates cyclic loads on the joints as they are thermally cycled during normal operation.

An SBC structure that has been subjected to accelerated thermal cycling (ATC) is shown in **Figure 2.** In this figure, the module is at the top and the card at the bottom; the card pad and part of the via and inner-plane structure are evident. The fatigue failure shown in this cross-section photomicrograph indicates cracking of the solder joint along the interface between the card pad and the eutectic fillet. The crack initiates on the side of the solder joint nearer the module center, and propagates along the interface of the solder fillet and the card pad until fracture occurs. For these structures, with an 0.86-mm module pad diameter and a 0.61-mm card pad diameter, the eventual fracture invariably occurred along the card-side interface.

To optimize reliability, packaging designers must be able to estimate accurately the effect of different sets of materials and geometry on fatigue life. This can be accomplished by using available solder reliability models (e.g., Coffin–Manson or its derivatives [2, 3]), all of which require as input some estimate of the cyclic distortions, or plastic strain, that the solder joint will experience.

This paper describes an analysis of an SBC assembly to determine the thermal distortions induced in the solder joints during ATC. Subsequently, the resulting strain in the SBC joints is used as a figure of merit to assess the dependence of reliability on various structural configurations. Finally, a reliability model is created by correlating the predicted distortions with the observed ATC lifetimes.

Approach

In C-4 technology, the finite element method has been applied to estimate the thermal strain sensitivity to geometric variables [4, 5]. These efforts view only a single solder joint with an applied translational (shearing) displacement. In the work described in this paper, models

are constructed which view the macro-level interactions that occur between the module and card, as well as the resulting micro-level deformations that occur in any single SBC solder joint within the array.

The modeling protocol employs both macro and micro models. The model geometries are constructed in CAEDS® [6]; the model solutions are generated using ANSYS® [7]. Ideally, one would prefer to construct a single model including an appropriate portion of both the module and the card, with sufficient detail in the solder ball regions of interest to accurately determine the plastic strain distribution. Such a model would, unfortunately, have to be quite large and would impose substantial computational requirements. To make the problem more feasible computationally, a macro/micro modeling approach is used.

In this approach, a relatively coarse macro model is constructed to represent the structural coupling between the module and the card, and to determine the major deformation modes that occur during thermal cycling. These thermal deformations (a shearing deformation and an axial deformation at a particular solder ball of interest) are used as input boundary conditions to a much more detailed micro model of a single SBC solder joint to determine the strain distribution within the joint.

The material properties used in the macro and micro models, excluding the solder materials, are shown in **Table 1**. Temperature dependence is included, and the materials are assumed to be linearly elastic.

The properties of the solder materials used in the models include the effects of elasto-plastic behavior, temperature, and strain rate. The tensile stress–strain data used in the models are shown in **Figure 3(a)** for eutectic solder and in **Figure 3(b)** for 90%Pb/10%Sn solder. These data were collected at 0°C and 100°C at a strain rate of 2×10^{-5} per second. This strain rate approximates the shear strain rate expected for SBC joints subjected to ATC (0–100°C, three cycles per hour, four-minute dwell at each temperature limit, linear temperature ramp). The finite element models are static, however, since no time-dependent effects are included.

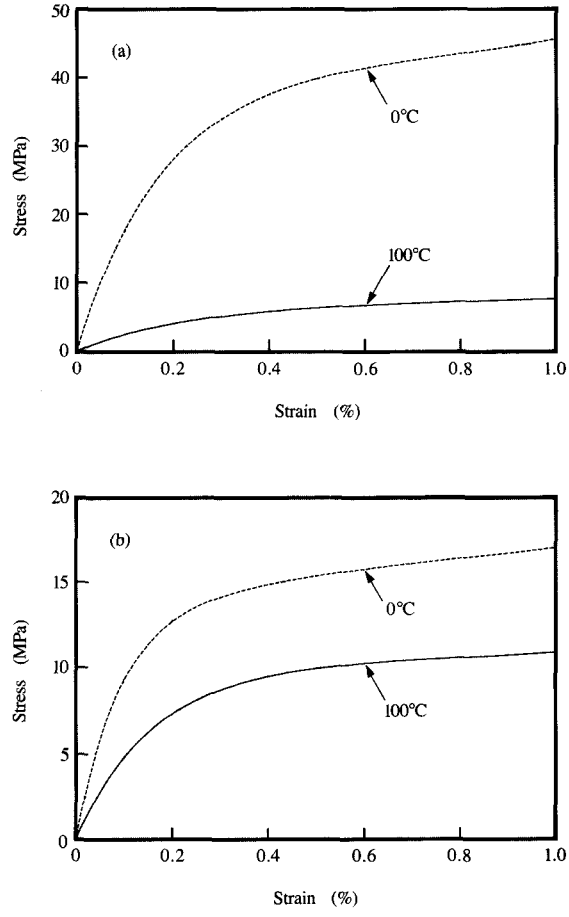

Figure 3

Tensile stress–strain relationship (strain rate = 2×10^{-5} per second) for (a) 63%Pb/37%Sn eutectic solder; (b) 90%Pb/10%Sn solder.

Table 1 Properties of materials used in models.

Material	*Elastic modulus E*		*Poisson's ratio ν at both 20°C and 100°C*
	at 20°C (10^{12} Pa)	*at 100°C* (10^{12} Pa)	
Ceramic	0.304	0.304	0.21
Molybdenum	0.321	0.315	0.30
Copper	0.126	0.102	0.29
FR-4	0.011	0.008	0.28

Macro and micro models

The macro models consist of thin plate elements representing the ceramic module and the FR-4 card, and beam elements that couple the module and the card. A group of beam elements that connects a single module pad to a card pad is termed an equivalent beam, and is designed to replicate the shear, bending, and axial-stiffness characteristics of a single SBC joint structure at its interfaces with both the module and the card (see **Figure 4**). The initial step is to determine the dimensions and material properties of the equivalent beams.

Before the equivalent beams can be defined, the nonlinear stiffness characteristics of the SBC solder structure must be estimated. This is accomplished using a micro-level finite element model. A typical micro model is shown in **Figure 5** for a module pad diameter of 0.86 mm

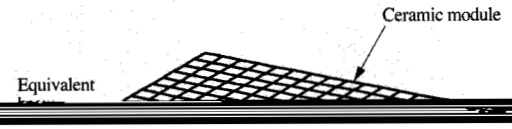

and a card pad diameter of 0.61 mm. Only half of the SBC joint structure need be modeled, because of symmetry. In this case, the symmetry plane passes through the center of the SBC joint and the module center, or neutral point, and

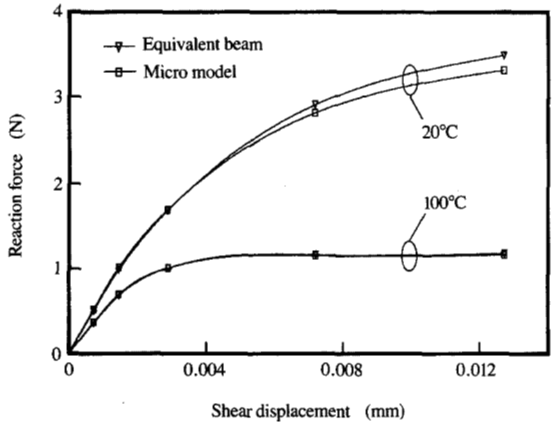

Figure 6

Micro model and equivalent beam reaction force to shear displacement.

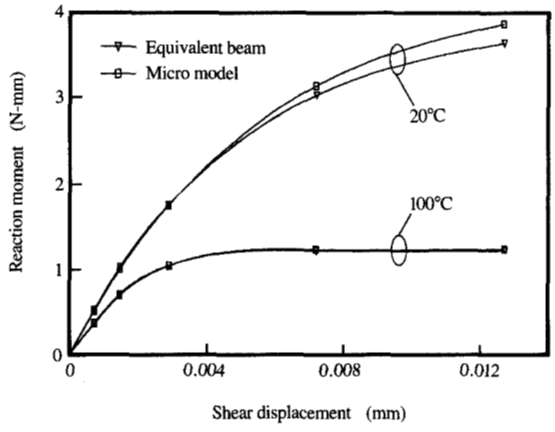

Figure 7

Micro model and equivalent beam reaction moment to shear displacement.

between the micro model and equivalent beam reactions is achieved, differing by at most 6% for the shear displacement, and by at most 16% for the axial displacement. The error is the penalty paid for replacing a 3000-element micro model with a five-element equivalent beam model.

A macro model for a 25-mm-square SBC module is shown in Figure 4. This three-dimensional model represents one quarter of a 19 × 19 array of solder balls spaced 1.27 mm apart (center-to-center) and consists of two layers of thin plate elements, one each for the module and card. Only one quarter of the structure is modeled because of symmetry. The module and card are coupled by a group of equivalent beam structures modeled with beam elements, the physical geometry and material properties of which are tailored, as previously described, to exhibit elasto-plastic responses to axial and simple shear deformations equivalent to those determined by the micro model.

Macro models simulate the major deformation modes that occur during thermal cycling. The outputs of the macro model are the relative displacements (shear, axial, and rotational) of each SBC connection in the array. These relative displacements are used as mid-plane boundary values for the micro model in order to determine the stress–strain distribution within the SBC structure for any chosen solder joint within the array, at any temperature. Plastic strains in the SBC structure can, therefore, be estimated as a function of structural configuration and material properties.

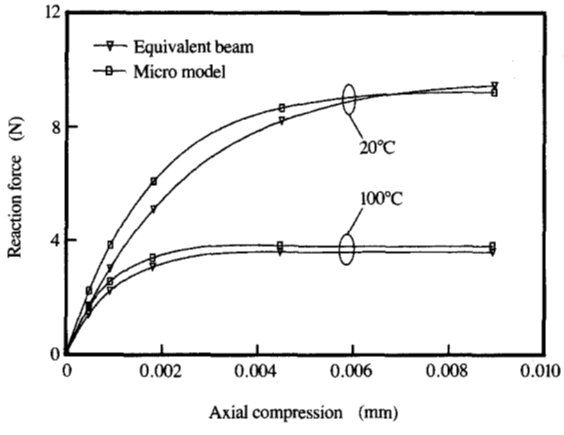

Figure 8

Micro model and equivalent beam reaction force to axial displacement.

Macro-level results

A series of nine temperature steps from 20° to 100°C was chosen to simulate the heating portion of an ATC cycle in the macro models. These temperatures are applied uniformly to all of the element nodes within the models. The solution of interest is at 100°C, but interim solutions must be generated at each of the applied temperatures to

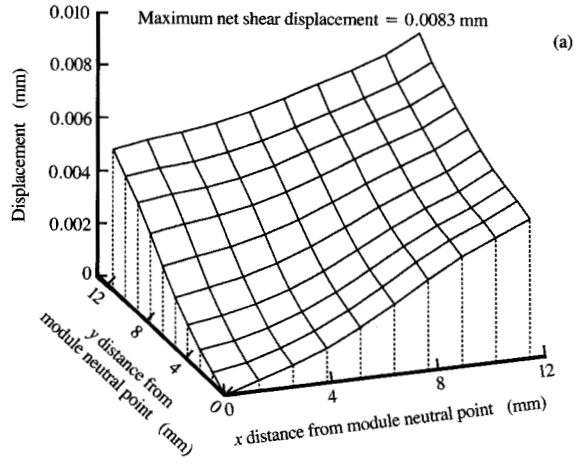

Figure 9

Deformations of 25-mm-square module at 100°C: (a) net shear translation; (b) net axial translation; (c) net rotation.

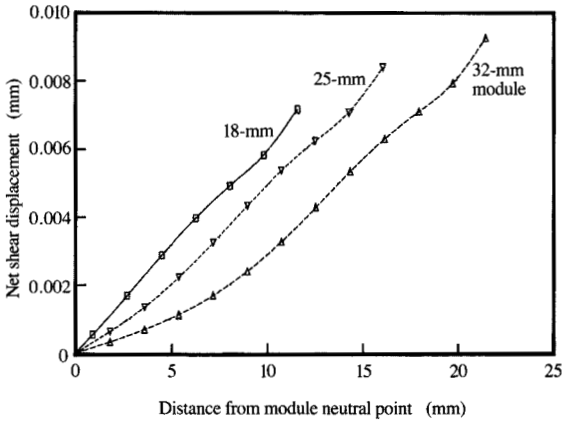

Figure 10

Net shear displacement along module diagonal at 100°C for three module sizes.

ensure numerical convergence, since the equivalent beams are defined elasto-plastically. The reference temperature (i.e., the temperature at which the thermal stresses are assumed to be zero) is 20°C, resulting in a simulated temperature change of 80°C.

The macro-level solutions at 100°C provide the global module and card deflections, from which the net SBC joint deflections (shear, axial, and rotational) are computed. The net SBC deflections are simply the relative motions of the module side of each SBC connection with respect to the card side, and are ultimately applied as boundary conditions to the micro model.

The three net deformation modes (shear, axial, rotational) for a 25-mm-square module are shown in **Figure 9** for the simulated temperature change of 80°C. (Note that for ease of visualization, the shear deformation mode is viewed from the module center, while the axial and rotational modes are viewed from a module corner.) The shear mode is effectively linear with respect to the distance from the module neutral point, with the maximum net shear displacement occurring at the corners (maximum distance to module neutral point). The maximum shear displacement for the 25-mm case is only 48% of the unconstrained shear that would occur were there no coupling between the module and card, indicating a substantial elastic contribution from the module and card.

The axial deformation is large along the module perimeter, is extreme at the module corners, and is minimal in the module interior. This result is analogous to that shown by Chen and Nelson [8] in their analysis of bonded elastic layers subjected to temperature variations.

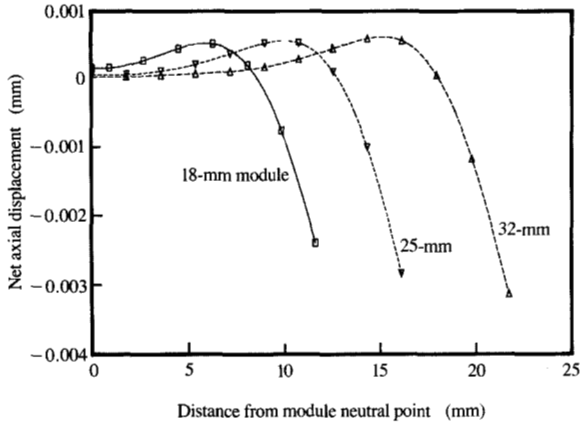

Figure 11

Net axial displacement along module diagonal at 100°C for three module sizes.

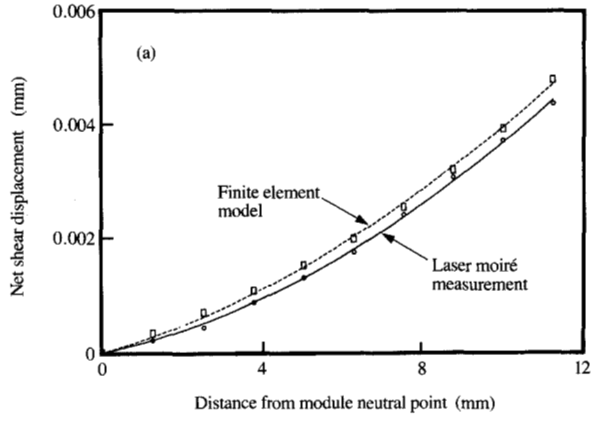

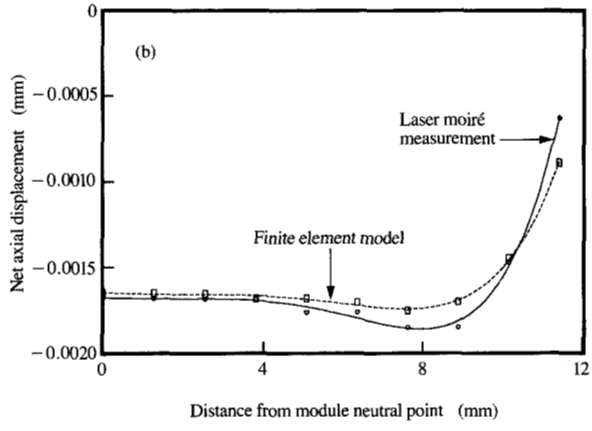

Figure 12

Deformation from finite element model compared with laser moiré interferometry measurement: (a) net shear displacement; (b) net axial displacement.

Note that at the corners the axial deformation magnitude is 35% of the net shear deformation.

The net rotation (rotation of the ceramic mid-plane with respect to the card mid-plane) is small. Although the gradients appear substantial, the displacements due to rotation are quite small compared to the shear and axial displacements. These small relative rotations are consistent with those observed by Hall [9].

SBC joints thus experience two major deformation modes during thermal cycling, a shear mode and an axial mode.

A comparison of the net shear and axial deformations for three different module sizes is shown in **Figure 10** and **Figure 11**, respectively. This comparison is viewed along the diagonal of the module, from the neutral point to the corner joint. Note that the maximum (corner) shear displacement is not a linear function of the maximum distance to the module neutral point (DNP), but approximates a square-root relationship. This suggests that reliability projections from a smaller module size to a larger one which assume a linear dependency on the maximum DNP, such as the Norris–Landzberg modified Coffin–Manson relationship [3], would significantly underestimate the fatigue reliability.

Guo et al. [10] describe the use of laser moiré interferometry to measure the thermal deformations in SBC assemblies. A macro-model finite element simulation of the devices measured by Guo et al., with an identical temperature excursion, was conducted. The simulated and measured shear deformation data are shown in **Figure 12(a)**; axial deformation data are shown in **Figure 12(b)**. Good agreement can be seen.

The net shear and axial deflections for any single SBC joint in the array are used as boundary conditions to the micro model. These are input as a series of displacement steps as required to ensure numerical convergence of the solution. In the work that follows, the corner joint (the highest-risk site in the array because of maximum shear and axial deflections) of a 25-mm module is examined.

Micro-level results

The equivalent plastic strain distribution within the eutectic solder of a corner joint of a 25-mm SBC assembly at 100°C is shown in **Figure 13.** In this model, the module

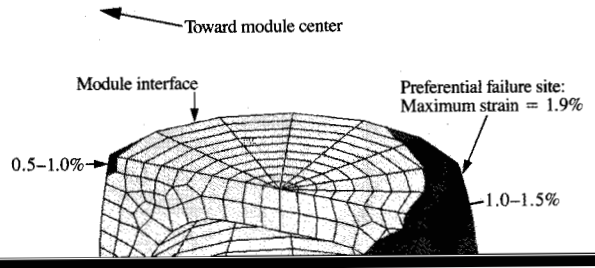

side cracking but invariably fracture along the interface between the card pad and eutectic fillet (see Figure 2). This failure mode is described by Banks et al. [1].

The preferential failure sites of a corner SBC joint, as shown in Figure 13, are due to the superposition of the stress states caused by the two major deformation modes. The shearing deformation mode creates a predominantly axial stress, as described by Robert and Keer [11] in their

Table 3 Structural optimization trial matrix.

Trial	D_m (mm)	D_c (mm)	$\bar{V}_m$	$\bar{V}_c$
1	0.51	0.51	0.50	0.50
2	0.86	0.86	0.50	0.50
3	0.86	0.51	1.00	0.50
4	0.51	0.86	1.00	0.50
5	0.51	0.51	0.50	1.00
6	0.86	0.86	0.50	1.00
7	0.86	0.51	1.00	1.00
8	0.51	0.86	1.00	1.00
9	0.86	0.86	1.00	0.75
10	0.86	0.51	0.50	0.75
11	0.51	0.86	0.50	0.75
12	0.51	0.51	1.00	0.75
13	0.69	0.69	1.00	1.00
14	0.86	0.69	0.75	1.00
15	0.69	0.86	0.75	1.00
16	0.69	0.51	0.50	1.00
17	0.69	0.86	0.50	0.50
18	0.86	0.51	0.75	0.50
19	0.51	0.69	1.00	0.50
20	0.51	0.69	0.50	1.00

previously described. The geometric variables of interest and their ranges are

- Module pad diameter D_m (0.51 mm $\leq D_m \leq$ 0.86 mm).
- Card pad diameter D_c (0.51 mm $\leq D_c \leq$ 0.86 mm).
- Normalized module-side solder volume $\bar{V}_m$ ($0.5 \leq \bar{V}_m \leq 1$).
- Normalized card-side solder volume $\bar{V}_c$ ($0.5 \leq \bar{V}_c \leq 1$).

The module-side and card-side solder volumes are normalized with respect to a reference volume defined to be that volume contained by a linear fillet extending from the edge of the module or card pad and tangent to the solder ball.

A four-variable quadratic designed experiment consisting of twenty trials was chosen, the trial matrix of which is shown in **Table 3**. For each trial in the matrix, a three-dimensional finite element micro model was constructed, with inputs consisting of shear and axial displacements based on solutions from macro models. Geometric assumptions include linear solder fillets, a fixed 0.94-mm standoff (card-to-module separation), and fixed 0.025-mm gaps (pad-to-ball separations).

The responses of interest are the maximum plastic strains within the module-side and card-side eutectic solder, and the maximum plastic strain within the solder ball.

The response surfaces from a regression analysis of the responses are shown in **Figure 14**, in which the sensitivity of the maximum strain to module pad and card pad diameters for constant solder volume is shown for both the eutectic- and ball-solder regions. The response surface in Figure 14(a), for peak eutectic solder strain, indicates a

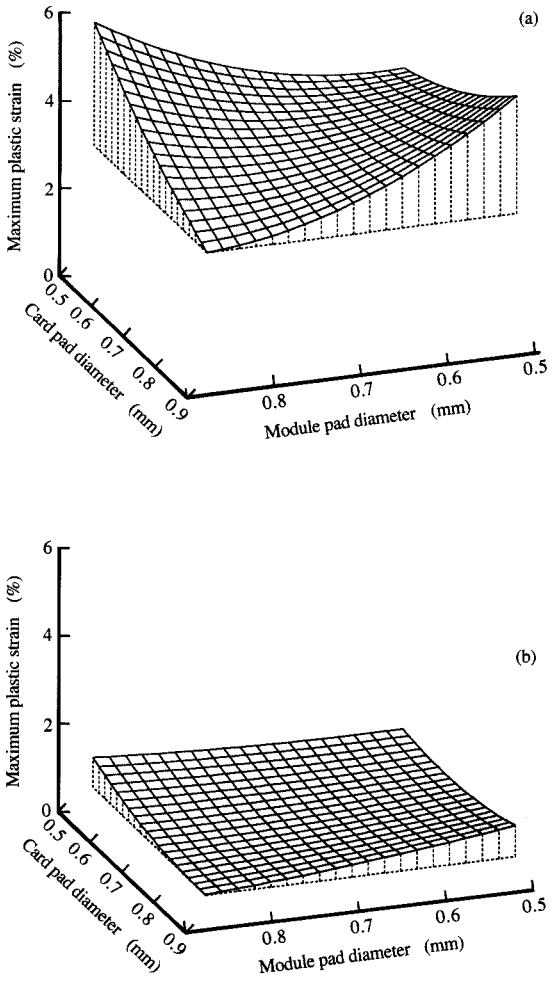

Figure 14

Sensitivity of maximum plastic strain to diameters of module pads and card pads with normalized module-side and card-side solder volume = 0.75: (a) in eutectic solder; (b) in solder ball.

trough of minimum strain for equal module pad and card pad diameters. (Depending upon the ratio of card pad diameter to module pad diameter, the maximum strain may occur on the card side or the module side.) Along this trough, maximum SBC-system eutectic solder strain is smaller for larger pad diameters. Hence, the optimum solution for minimizing peak SBC system eutectic solder strain is to use equal module pad and card pad diameters, with both as large as physically possible. This conclusion is the same as that described by Ohshima et al. [13], Kamei and Nakamura [14], and Lin et al. [15] in their analytic investigations of flip-chip thermal fatigue.

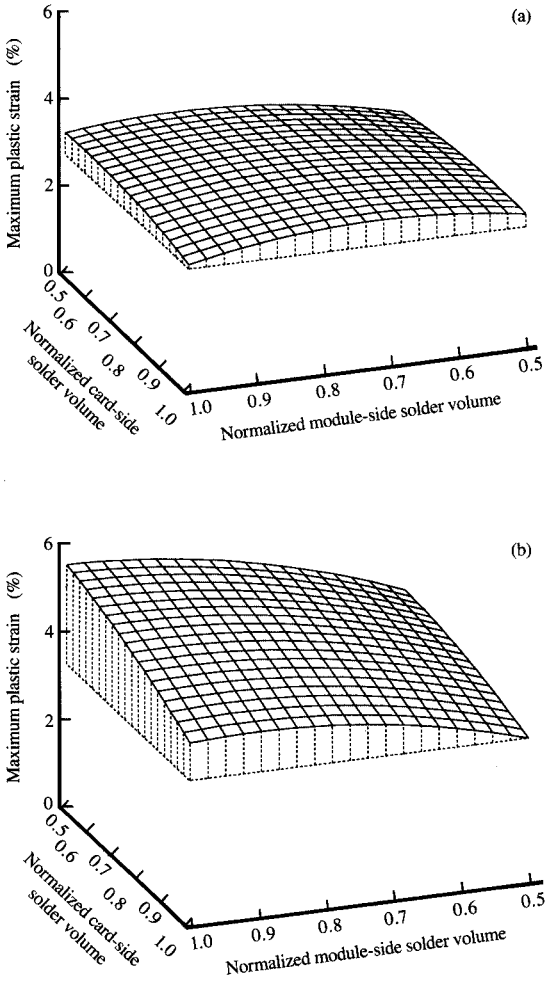

Figure 15

Sensitivity of maximum plastic strain to normalized module-side

upper limit of approximately 0.71 mm on the card pad diameter (constrained by plating tolerances, the SBC pitch, and the required number of lines per channel) and an 0.81–0.86-mm lower limit on the module pad size due to drilling considerations.

The strain sensitivity of the solder ball to module and card pad diameter is shown in Figure 14(b). The shape is similar to that of Figure 14(a), but the maximum strain amplitude is substantially below that experienced by the eutectic solder. Clearly, the eutectic solder strains dominate, and minimizing peak eutectic solder strain effectively minimizes SBC-system strain.

The sensitivity of the maximum eutectic solder strain to module and card solder volumes for two different pad-diameter sets is shown in **Figure 15**. Strain within the eutectic solder is essentially insensitive to the normalized solder volume on both the module side and the card side, if the module-side and card-side pad diameters are equal or close to equal, as shown in Figure 15(a) for the case of D_m = 0.76 mm, D_c = 0.76 mm. This is an extremely important observation, since an SBC structure optimized for minimum system strain also offers the important advantage of minimizing the sensitivity to assembly process variables, specifically solder volume. This results in a much more robust and easily controlled assembly process.

As the pad diameters become unequal, however, solder volume does influence the maximum eutectic solder strains, as shown in Figure 15(b) for the case of D_m = 0.86 mm, D_c = 0.61 mm. For unequal pad diameters, maximum eutectic strain can be minimized by reducing the solder volume on the larger pad and increasing the volume on the smaller pad. The overall influence of solder volume is, however, less pronounced than that of module pad and card pad diameters.

Reliability model

suggested by Coffin and Manson [2], and closer still to the value of −1.9 suggested by Norris and Landzberg [3].

This power-law relationship is the basis of a reliability model used to estimate the influence of various structural modifications and assembly-process variables on fatigue reliability. The ATC cycles to failure are used as a basis of comparison; actual performance is a function of operating environment, cycle frequency, and other factors, and can be estimated using a modified Coffin–Manson approach [18].

Conclusions

A procedure was described whereby the thermal strain distribution within an SBC joint can be estimated through a series of macro and micro finite element models.

Equivalent beam structures were described which effectively duplicate the force and moment coupling experienced between the SBC module and card.

Major conclusions are the following:

1. There are two dominant deformation modes associated with SBC joints, a shear mode and an axial mode.
2. These deformation modes are most severe at the module corners, making corner joints the most likely to fail.
3. The preferential failure locations of an SBC joint are the outboard module-side eutectic solder and the inboard card-side eutectic solder, both locations consistent with observed failures on ATC-cycled assemblies.
4. These preferential failure locations within a corner joint of SBC assemblies are due to the axial deformation resulting from bending of the card–module assembly. The uniform compressive stress (at high temperature) resulting from bending is additive along the outboard module-side and inboard card-side eutectic solder joints, but is subtractive along the other diagonal of the joints.
5. SBC eutectic solder strain can be minimized by designing the module pad and card pad diameters to be as close to each other and as large as possible, consistent with other constraints imposed by manufacturing.
6. Such an optimal SBC structure provides the most robust assembly process, i.e., one substantially insensitive to moderate variations in solder volume.
7. Finite element model estimates of the eutectic solder plastic strain correlate well with measured accelerated thermal cycle testing fatigue data. These models, therefore, provide an excellent vehicle for predicting the influence of structural modifications on fatigue reliability.
8. Peak strains in the solder ball are substantially lower than those in the eutectic solder fillets; hence, there is a potential reliability enhancement based on redistributing the SBC joint compliance and allowing the ball to accommodate more strain.

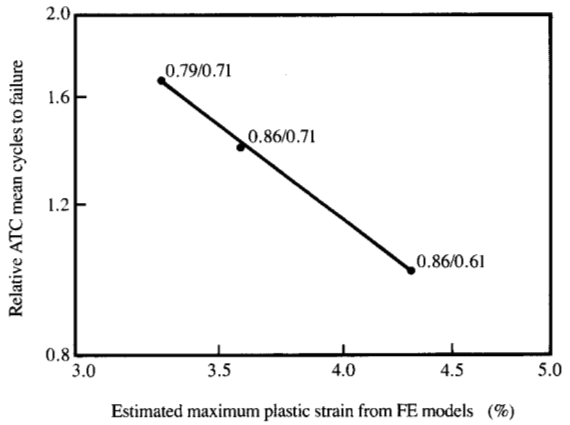

Figure 16

SBC reliability model for 25-mm module. The combination of pad diameters (in mm) is shown for each point as module/card. The straight line corresponds to the following relation: relative mean ATC cycles to failure = 16.28 × (maximum plastic strain)$^{-1.91}$.

Acknowledgments

I thank Tom Caulfield and Marie Cole of IBM East Fishkill for providing the material properties data for eutectic and 90%Pb/10%Sn solder, and Stan Wheeler of IBM Austin for statistical analysis support.

References

1. M. D. Ries, D. R. Banks, D. P. Watson, and K. G. Hoebener, "Attachment of Solder Ball Connect (SBC) Packages to Circuit Cards," *IBM J. Res. Develop.* **37**, 597–608 (1993, this issue).
2. S. S. Manson, *Thermal Stress and Low-Cycle Fatigue*, McGraw-Hill Book Co., Inc., New York, 1966, pp. 125–192.
3. K. C. Norris and A. H. Landzberg, "Reliability of Controlled Collapse Interconnections," *IBM J. Res. Develop.* **13**, 266–271 (1969).
4. E. A. Wilson and E. P. Anderson, "An Analytical Investigation into Geometric Influence on Integrated Circuit Bump Strain," *Proceedings of the 33rd Electronic Components Conference*, 1983, pp. 320–327.
5. W. M. Sherry, J. S. Erich, M. K. Bartschat, and F. P. Prinz, "Analytical and Experimental Analysis of LCCC Solder Joint Fatigue Life," *Proceedings of the 35th Electronic Components Conference*, 1985, pp. 81–90.
6. *CAEDS Graphics Finite Element Modeler User's Guide*, Version 3, Release 2, IBM Corporation, 1990.

7. *ANSYS Engineering Analysis System User's Guide*, Revision 4.4, Swanson Analysis Systems, Inc., Houston, PA, 1989.
8. W. T. Chen and C. W. Nelson, "Thermal Stress in Bonded Joints," *IBM J. Res. Develop.* **23**, 179–188 (1979).
9. Peter M. Hall, "Forces, Moments, and Displacements During Thermal Chamber Cycling of Leadless Ceramic Chip Carriers Soldered to Printed Boards," *IEEE Trans. Components, Hybrids, Manuf. Technol.* **CHMT-7**, 314–327 (1984).
10. Y. Guo, C. K. Lim, W. T. Chen, and C. G. Woychik, "Solder Ball Connect (SBC) Assemblies Under Thermal Loading: I. Deformation Measurement via Moiré Interferometry, and Its Interpretation," *IBM J. Res. Develop.* **37**, 635–647 (1993, this issue).
11. M. Robert and L. M. Keer, "An Elastic Cylinder with Prescribed Displacements at the Ends—Asymmetric Case," *Quart. J. Mechan. Appl. Math.* **40**, 365–381 (1987).
12. G. E. P. Box, W. G. Hunter, and J. S. Hunter, *Statistics for Experimenters—An Introduction to Design, Data Analysis, and Model Building*, John Wiley & Sons, Inc., New York, 1978.
13. M. Ohshima, A. Kenmotsu, and I. Ishi, "Optimization of Micro Solder Reflow Bonding for the LSI Flip Chip," *Proceedings of the International Electronics Packaging Conference*, 1982, pp. 481–488.
14. T. Kamei and M. Nakamura, "Hybrid IC Structures Using Solder Reflow Technology," *Proceedings of the 28th Electronic Components Conference*, 1978, pp. 172–182.
15. P. Lin, J. Lee, and S. Im, "Design Considerations for a Flip-Chip Joining Technique," *Solid State Technol.* **13**, 48–54 (1970).
16. L. S. Goldmann, "Geometric Optimization of Controlled Collapse Interconnections," *IBM J. Res. Develop.* **13**, 251–265 (1969).
17. L. S. Goldmann and P. A. Totta, "Area Array Solder Interconnections for VSLI," *Solid State Technol.* **26**, 91–97 (1983).
18. D. Jeannotte, L. Goldmann, and R. Howard, "Package Reliability," *Microelectronics Packaging Handbook*, R. Tummala and E. Rymaszewski, Eds., Van Nostrand Reinhold, New York, 1989, Ch. 5, pp. 295–299.

Received December 14, 1992; accepted for publication January 26, 1993

John S. Corbin *IBM Advanced Workstations and Systems Division, 11400 Burnet Road, Austin, Texas 78758 (CORBIN at AUSVMV).* Mr. Corbin received his B.S. and M.S. degrees in mechanical engineering from the University of Texas at Austin in 1972 and 1974, respectively. He joined IBM in 1974 and spent ten years in printer development, working primarily in the area of motion control. This was followed by six years in the Systems Technology Division Packaging Laboratory in Austin, applying finite element techniques in the area of mechanical-packaging reliability. He is currently a Senior Engineer in the Advanced Workstations and Systems Division, where his interests relate to system-packaging reliability. Mr. Corbin is a registered professional engineer in the state of Texas.